International Journal of Computing and Digital Systems
2025, VOL. 17, NO. 1, 1–14

http://dx.doi.org/10.12785/ijcds/1570996365

Classification of Osteoporotic X-ray Images using Wavelet Texture Analysis and Machine Learning

Sai Kiran K S[1,2] and Anu Shaju Areeckal[3,*]

[1]*Department of Bioinformatics, Manipal School of Life Sciences, Manipal Academy of Higher Education, Manipal 576104, India*
[2]*Novo Nordisk GBS, Cignus, Whitefield, Bengaluru, Karnataka 560066, India*
[3]*Department of Electronics and Communication Engineering, Manipal Institute of Technology, Manipal Academy of Higher Education, Manipal 576104, India*
[*]*Corresponding author*

Received 5 February 2024, Revised 14 January 2025, Accepted 14 January 2025

Abstract: Osteoporosis, a disorder defined by decreased bone mineral content and changes in bone microarchitecture, poses a challenge for accurate classification using X-ray images. This paper aims to extract texture features from calcaneal radiographs and select the best texture features which can be used to train the machine learning classifier models for the detection of osteoporosis. This work is based on multiresolution analysis and microstructural analysis to characterize trabecular bone microarchitecture from calcaneal radiograph. The image is transformed to extract the feature details using a two-level wavelet decomposition. Structural texture methods such as Local Binary Pattern, fractal dimension and Gabor filter are applied to the wavelet decomposed images. The most discriminating texture features are selected using independent sample t-test and feature selection methods. Machine learning models are constructed by training the classifiers using the best texture features to classify healthy images from osteoporotic images. The effectiveness of the proposed approach is evaluated using a public challenge dataset comprising calcaneal radiographic images. Notably, the best classification is obtained with k-Nearest Neighbour trained with the features selected using forward feature selection, with an accuracy rate of 78.24%. The results indicate the potential of the proposed approach as a possible alternative tool for low cost screening of osteoporosis.

Keywords: Osteoporosis, Health care, Machine learning, Texture analysis, Classification

1. Introduction

Osteoporosis is a prevalent metabolic disease characterized by reduced bone strength, primarily defined by bone mineral density (BMD). Osteoporosis is operationally recognized by the World Health Organization as having a BMD that is 2.5 standard deviations or more below average (T-score less than -2.5) [1]. The global impact of osteoporosis is significant, with an estimated 200 million individuals affected by the condition. The International Osteoporosis Foundation's statistics show the prevalence of osteoporotic fractures are all around the world. According to statistics, one in three women aged 50 or older and one in five males will have an osteoporotic fracture over their lifetime [2]. In India, the prevalence of osteoporosis among adults is estimated to be 22.9 percent. The prevalence is higher in females (26.3 percent) compared to males (10.9 percent), surpassing the global prevalence of 18.3 percent [1].

Osteoporosis poses a significant medical and socio-economic threat as it leads to a systemic deterioration of bone mass and microarchitecture, increasing the susceptibility to fragility fractures. In individuals with osteoporosis, the production of new bone fails to keep pace with the loss of old bone, resulting in decreased BMD. This reduced BMD makes even minor stresses potentially fracturing, and the associated chronic pain severely limits daily activities [3]. Common sites for osteoporosis-related fractures include the hip, wrist, and spine [4].

Various techniques, such as High-Resolution Peripheral QCT (HR-pQCT), Magnetic resonance imaging (MRI), Quantitative Computed Tomography (QCT), Dual X-ray Absorptiometry (DXA), digital X-ray radiogrammetry (DXR) and quantitative ultrasound (QUS) are employed for diagnosing osteoporosis [5]. Zhao et al. [6] utilized QCT and MRI scans of 222 subjects to develop a deep learning based segmentation model and radiomic pipeline to classify osteoporotic from healthy cases. Accuracy of 84.4% was obtained. A study on detection of osteoporosis using CT scans of hip joints of 474 people showed that including

E-mail address: saikiranks14@gmail.com, anu.areeckal@manipal.edu

clinical features of patients with radiomic features helps in improved accuracy of 88.2% [7]. Another study utilized CT, dual X-ray and radiographs for classification of osteoporotic people from healthy ones, using a convolutional neural network based on channel boosting and transfer learning techniques [8]. This method showed improved accuracy over existing models. The above mentioned imaging modalities have a few drawbacks. QCT has a high cost, radiation, increased radiation exposure and complex scanning procedure [9]. MRI is expensive and time consuming Ultrasound has an increased discrepancy between devices and hence is useful for screening only [9].

A recent study showed the potential of photoacoustic physicochemical analysis for bone health assessment on rabbit bone models [10]. This method is non-invasive and non-ionizing and can simultaneously capture the metabolic as well as structural details of the bone. However, this study was done as ex-vivo experiment and needs further research in vivo in bones with soft tissue, before it can be used in clinical settings.

DXA is regarded as the gold standard technique for BMD assessment; however, its availability is limited in low-income economies, and the cost of scans is high [11]. DXA is a large and bulky standalone device that requires rigorous quality control [9]. Cortical radiogrammetry, a cost-effective technique using radiographs, has proven useful in detecting bone loss. For identifying various bone disorders, the advanced cortical radiogrammetric method known as Digital X-ray Radiogrammetry (DXR) has been widely explored [12]. Cortical radiogrammetry does not examine the texture of trabecular bone, but only evaluates cortical bone characteristics. Before an apparent decrease in cortical bone is seen, osteoporosis first affects the trabecular bone structure. Additionally, measuring BMD alone is not a reliable way to predict fracture risk. Non-BMD variables like microarchitecture can also be used to describe the quality and strength of bone. Given the expense and limitations of existing diagnostic techniques, there is a pressing need to develop a low-cost device that utilizes bone microarchitecture for early detection and diagnosis of osteoporosis.

Imaging is a potential way to support the diagnosis and aid the practitioner in making decisions. Texture analysis and classification enables an easy and less intrusive technique to describe the micro-architecture of the bone on X-ray images. It helps assess the risk of bone fracture and aid in the early diagnosis of osteoporosis. Studies have demonstrated the value of texture analysis of trabecular bone in the diagnosis and early detection of fractures associated with osteoporosis.

The objective of this paper is to develop a low cost and feasible screening tool for the classification of osteoporosis using calcaneal radiographic images. The advantages of using calcaneal radiographs lies in the fact that the degradation in the trabecular bone is better characterized by pressure points such as heels, and it is a site which can be easily imaged in elderly people, especially those with morbid conditions.

The main contributions of our paper are as follows. 1. A thorough experimentation on the effectiveness of using discrete wavelet decomposed images for texture feature extraction is explored. 2. The impact of using feature selection methods such as statistical analysis and forward feature selection, on the detection rate of osteoporosis is investigated. 3. The best classification model is developed by training three classical machine learning algorithms, namely support vector machine (SVM), k-Nearest neighbour (KNN) and Random forest (RF), with different texture features. The final framework can be potentially used as a screening tool for osteoporosis.

2. Related Work

Recent studies have shown the potential of using machine learning techniques on imaging modalities with low cost and low scanning time, for a more feasible detection of osteoporosis [9]. Several works reported the ability to distinguish between osteoporotic and healthy participants using trabecular texture characteristics from radiographs of different regions-of-interest, such as calcaneal, knee, spine, chest, tibia, periapical radiographs, etc. In a study of 104 lumbar spine radiographs and 174 calcaneal radiographs, texture features of bone were extracted and Davies–Bouldin index and Neighborhood component analysis were employed for feature engineering [13]. The best six features trained on a support vector machine achieved accuracy of 85.1% for osteoporosis detection in spine and 76.7% in calcaneus. Patil et al. [14] extracted Pyramid Histogram of Orientation Gradient features from lumbar vertebrae L1-L4 and trained neural network with L2 regularization for osteoporosis classification. An accuracy of 99.34% was obtained.

Du et al. [15] used artificial neural network (ANN) for prediction of osteoporotic fracture in femoral neck in the elderly and achieved accuracy of 95.83%, as compared to SVM with accuracy of 62.50%. Another study on femur bone radiographs employed maximum response filter at different scales on sub-bands of 2D Discrete Wavelet Transform [16]. F1-score and accuracy of 96.54% and 95.45% was achieved, respectively. Massatith et al. [17] did an extensive investigation on 2445 X-ray images of hip and thorax regions and trained KNN and convolutional neural network (CNN) models to achieve a test accuracy of 78.57% and 97.57%, respectively. A study on machine learning classifiers trained with 93 radiomic features extracted from 565 pelvic X-ray images showed that a combination of the texture features with clinical parameters showed a higher area under the Receiver Operating Characteristic curve (AUC) of 0.68 for classification of healthy and osteoporotic subjects [18].

Another potential site for osteoporosis detection is the

tibia, from which histogram and texture features have been extracted and trained using SVM to obtain an accuracy of 83.6% [19]. Widyaningrum et al. [20] utilized periapical radiographs to segment 120 regions-of-interest using colour histogram and to classify into healthy and osteoporotic subjects using machine learning classifiers. K-means segmentation with multi-layer perceptron classifier achieved best accuracy of 90.48%. A recent review on various literature on osteoporosis reported that the accuracy of osteoporosis classification algorithms ranged from 66.1% to 97.9% [21].

This paper focuses on utilizing calcaneal radiographs to classify osteoporosis. The calcaneus is a weight-bearing bone with a high trabecular content. This makes it ideal for detailed texture description related to bone degradation. It is a more accessible and practical imaging site for the morbid elderly people. Various related work on classification of osteoporosis using calcaneal radiographs are discussed below.

Harrar et al. [22] used calcaneal radiographs of 174 women, which included 87 images in both healthy and osteoporotic category. An effective fractal dimension estimator known as the anisotropic piecewise Whittle estimator was combined with an anisotropic fractional Brownian motion model in their oriented analysis technique. The work obtained an accuracy of 71.8% with 72% sensitivity, 71% specificity and AUC of 78%. Riaz et al. [23] used calcaneal TCB dataset, which included 58 images in both healthy and osteoporotic categories. The work made use of Gabor filter bank, which is made up of filters with four different scales and four orientations. The one dimensional Local Binary Pattern (LBP) histograms are then acquired. LBPs calculated by taking into consideration eight neighbors with one pixel separation, obtained an accuracy of 72.71%.

Palanivel et al. [24] used calcaneal TCB dataset, which included 58 images in both healthy and osteoporotic categories. Multifractal analysis has been utilized to describe the bone texture. Here, local texture differences are effectively described by a set of local fractal dimensions rather than a single global fractal dimension. The effectiveness of the box-counting approach and the regularization dimension method are evaluated. The performance is enhanced by combining both the characteristics. The work obtained accuracy of 55% with 59% sensitivity and 52% specificity.

Zehani et al. [25] used Region of Interest (ROI) taken from the trabecular bone images of individuals with varied ages and osteoporotic diseases using X-rays. They developed a fractal model that employs the differential box-counting method to calculate the fractal dimension (FD), which is done post image preprocessing step that ensures a reliable estimation approach and obtained a better result with p-value < 0.05.

Zheng et al. [26] presented sparse representation-based technique for distinguishing healthy from diseased states using medical imaging patterns. Two classifiers based on log likelihood function and maximum a posteriori probability were developed. In order to handle the approximation problem's irregularities and construct a classifier ensemble that would produce more precise numerical answers than traditional sparse assessments of the entire spatial domain of the pictures, a spatial block decomposition approach was suggested. The work obtained accuracy of 67.8% with specificity 65.5% sensitivity 70.1% and AUC of 65%.

Palanivel et al. [27] used calcaneal TCB dataset, which contains 58 images in both healthy and osteoporotic categories. Multifractals are used in their research to describe the trabecular bone microstructure. In order to assess the overall regularity of the pixels, Hausdorff dimensions are first calculated for each Holder exponent. Finally, the Hausdorff dimensions are used to calculate lacunarity. The work reported accuracy of 59% with 59% sensitivity and 59% specificity.

Bouzeboudja et al. [28] used calcaneal X-ray image dataset, which contains 87 images in both normal and osteoporosis categories. The proposed method follows different steps. The radiographic images are binarized after going through a median filtering stage of preprocessing. After computing the multi-fractal spectrum, numerous features are obtained to describe the microarchitecture of the trabecular bone. Finally, the two groups of osteoporotic as well as healthy radiographs are classified using the obtained features. The work achieved accuracy of 98.01%, with 97.26% sensitivity, 98.78% specificity and AUC of 98.37%. Mebarkia et al. [29] applied Histogram of Gradient (HOG) and LPQ to calcaneal bone texture images obtained from Gabor filter banks whose parameters are optimized using bat-inspired algorithm, and achieved accuracy of 89.66%.

Recent studies have used deep learning approach for classification of X-ray images as osteoporotic or healthy [30],[31],[32]. Lindsey et al. [30] used deep learning for classification of fractured and healthy wrist radiographic images. The work obtained 93.9% sensitivity, 94.5% specificity and AUC of 97.5%. Kumar et al. [31] attained testing accuracy of 82% and validation accuracy of 84% on untrained test radiographic images. Harris and Makrogiannis [32] obtained an AUC of 76.80% and accuracy of 72.67%.

A modified U-net with residual block and skip connections was used to categorise subjects into normal osteopenia and oteoporosis using radioraphs [33]. An accuracy of 86.6% was achieved. Basavaraja et al. [34] applied image processing techniques such as active shape and appearance models, Gray level co-occurrence matrix (GLCM), median ternary and mean local gradient patterns, on knee radiographs. An ensemble of deep learning models achieved accuracy of 94.8%.

Patil et al. [35] trained a CNN with Laws texture features on 162 spine X-ray images, and obtained 100% accuracy. However, the work used a small dataset and tends to overfit. A modified CNN with controllable feature layer was

trained on hip images of 1730 patients [36]. Inclusion of clinical parameters resulted in AUC of 96%. Kim et al. [37] combined texture features with deep features and clinical parameters to obtain an increased AUC of 0.95, as compared to just using deep features alone (AUC of 0.92).

Hidjah et al. [38] hypertuned deep CNN using dental periapical radiographs and achieved test accuracy is 92.5%. Tsai et al. [39] developed deep learning model using 48353 chest X-rays and achieved AUC of 89.2%. A study using 846 panoramic radiographs for training YOLOv5 deep model and achieved F1-score of 99.3% [40].

Tassoker et al. [41] used transfer learning on popular deep learning models to classify panoramic radiographs of women into healthy, osteopenia and osteoporosis. GoogleNET showed the best results for healthy and non-healthy cases with accuracy of 92.79%, while AlexNet showed accuracy of 98.56% for healthy and osteoporotic classes, leaving out the osteopenia cases. It was reported that inclusion of osteopenia cases degraded the accuracy of the ensemble classifiers. Another study used eight pre-trained models to classify X-ray images [42]. VGG-16 gave the best results with accuracy of 86.36%.

Although deep learning techniques show higher accuracy than classical machine learning, however, deep learning techniques are heavy, computationally extensive to train, and requires a large database to ensure robustness and clinical applicability of the model.

The proposed work in this paper aims to enhance the accuracy and precision of osteoporosis diagnostic tools by leveraging texture features extracted from calcaneal radiographs. By identifying significant texture features, this paper intends to train machine learning models and develop a classifier that can effectively differentiate between healthy and osteoporotic images. This approach holds promise in improving the diagnostic capabilities and overall effectiveness of osteoporosis diagnosis.

3. Proposed Methodology

The proposed approach operates using different stages, as shown in Figure 1. Prior to using a median filter to reduce noise content, the images are first preprocessed by increasing contrast using Contrast Limited Adaptive Histogram Equalization (CLAHE). Then, using various feature extraction approaches, texture features are obtained to characterize the trabecular bone microarchitecture. Feature selection strategies are used to choose the relevant features. Finally, osteoporotic and healthy radiographs are classified by training machine learning classifiers using the retrieved features.

A. Dataset

The images used in this paper are obtained from the TCB challenge dataset, released by International Society for Biomedical Imaging (ISBI) in 2014. This challenge involves applying texture analysis to classify osteoporotic patients from normal individuals based on X-ray images. The dataset consists of radiographs of calcaneal bone of two different population. Patients with osteoporosis and healthy individuals constitute the reference population. The images are of 400×400 pixels in 16-bit format. There are 58 images each of osteoporotic and healthy people in the dataset. Figure 2 shows some sample images from the dataset.

B. Preprocessing

Bone X-ray scans reveal striking similarities between osteoporotic patients and healthy individuals. Each image is initially preprocessed in order to enhance image quality and improve the proposed technique's capacity to distinguish between two separate classes. A nonlinear median filter of size 3×3 is used on each grayscale image to eliminate the impulse noise without changing the frequencies, which are important for classifying osteoporosis. The impulsive noise created during acquisition is primarily eliminated by the median filter. The image intensity levels are then normalized in order to improve the contrast.

C. Feature Extraction

Gravity (tension) as well as walking force (compression), which are applied to the heel, cause anisotropic qualities in the bone structure. The bone structure has anisotropic characteristics as a result of these forces. Additionally, normal (dense) and osteoporotic bones exhibit different levels of granularity, emphasizing the importance of multiresolution analysis that considers orientation and scale variations, as well as microstructural analysis [23]. To characterize the trabecular bone structure, various analysis methods based on fractal, structural, and texture transforms are employed.

In this proposed method, texture feature extraction methods are utilized to analyze the trabecular features of the calcaneal bone X-ray images. Specifically, we employ structural features such as local binary pattern, fractal features such as fractal dimension, and transform-based features including Gabor transform and discrete wavelet transform. These features enable a comprehensive analysis of the trabecular bone structure, considering its unique properties and variations.

The Local Binary Pattern (LBP) approach utilize the statistical distribution of local patterns to characterize textures. It assigns labels to pixels by comparing their intensity values with the surrounding pixels and it computes a rotation-invariant metric known as the uniformity measure U. Patterns are given the LBP code if their U value is less than 2, indicating that the center pixel is labeled as uniform [43]. Three different neighbor configurations are considered, namely 8, 16, and 24, with respective pixel spacing of 1, 2, and 3. Energy and entropy are then extracted from the resulting LBP images, generating a feature vector with six features for each preprocessed image.

Gabor transform (GT) is employed to represent and differentiate textures by examining the presence of specific

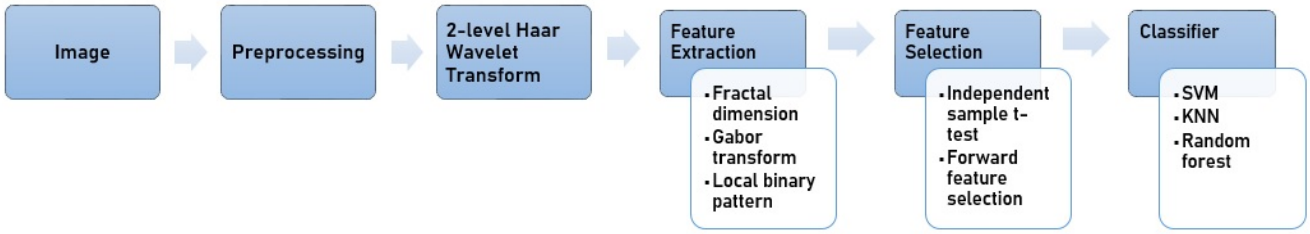

Figure 1. Methodology of the proposed work: The raw image is preprocessed and features are extracted using different texture analysis techniques, followed by feature selection. Classifiers are trained with the best texture features to classify healthy and osteoporotic images.

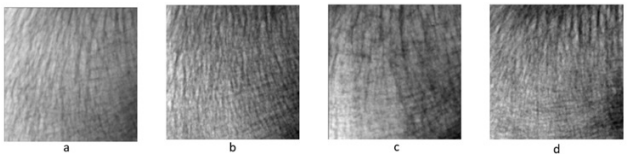

Figure 2. Calcaneal radiographs obtained from the dataset: (a) and (b) are calcaneal radiographs of class 0 category, and (c) and (d) are calcaneal radiographs of class 1

frequency content in the localized area surrounding the point or region of interest [23]. Gabor filters are applied, resulting in Gabor images of different scales and orientations. Mean and standard deviation features are extracted from the set of Gabor filters with various orientations and frequencies, resulting in a feature vector with 16 features for each preprocessed image.

Fractal Dimension (FD) analysis, suitable for evaluating bone microstructure on radiographs, utilize the box-counting algorithm to characterize trabecular bone patterns [44]. Hurst coefficients are extracted from each image, generating a feature vector containing four coefficients.

Discrete wavelet transform (DWT) decomposes the images into four sub-images by convolving them with specific filters. These sub-images capture frequency information across various frequency ranges [45]. In this work, two-level decomposition is applied to each preprocessed image, resulting in a set of seven sub-images as shown in Figure 3.

LBP, GT, and FD analysis are then applied to all seven sub-images, generating a feature vector with 96 features. This feature extraction process is repeated for all preprocessed images, resulting in a comprehensive set of features that capture different aspects of the trabecular bone structure and texture.

D. Feature Selection

The extracted feature vectors may contain features that are not significant. It is important to remove any extraneous features since they might lower classification accuracy and make the classifier more complicated. It is possible to choose the most important and dominating features using a variety of feature selection techniques. In this paper, an independent sample t-test and forward feature selection

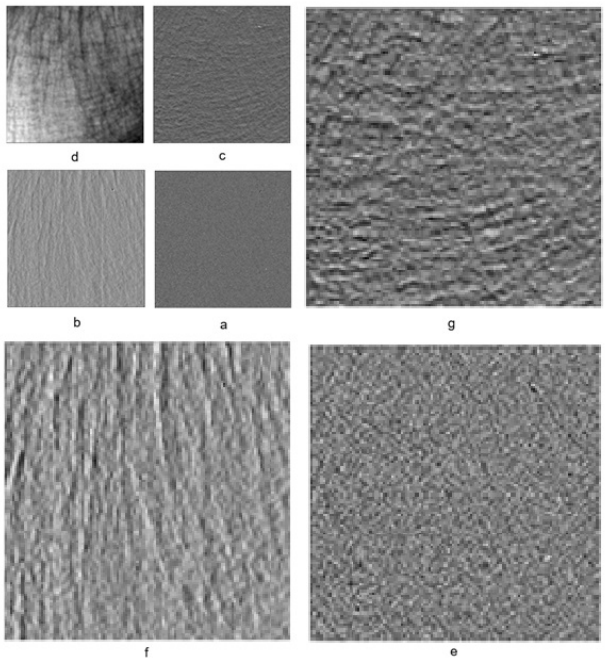

Figure 3. Two-level Wavelet Decomposition: (a) High High (HH), (b) High Low (HL), (c) Low High (LH), and (d) Low Low (LL) sub-band images of the second level of Haar decomposition. (e)-(g) are the HH, HL and LH sub-band images of the first level, respectively.

method are used for feature selection.

In this work, the significance value, p-value, of each feature obtained is calculated using an independent sample t-test. According to the test, features with a p-value of 0.05 or less are deemed to be significant [25]. Hence the features with significance value, p-value, of 0.05 or less are considered to form feature vectors, which are then used for training classifiers.

Forward feature selection method is an iterative process where features are progressively added to a subset based on their impact on the performance of a machine learning model. It starts with an empty set and successively adds features that improve model performance until a stopping criterion is met. The process evaluates different feature subsets and selects the one that yields the best model perfor-

mance [46]. We use this method to obtain a feature vector containing dominant features showing the best accuracy amongst all others.

E. Classification

The different classifiers used are SVM, KNN and RF classifiers. For KNN, various values of nearest neighbours are considered. The number of nearest neighbours are chosen to be six, as it gave the best results. For the RF classifier, the number of estimators varies depending on the number of features. If the features are less than 15, 10 estimators are used, while if the features are more than 25, 100 estimators are used. The choice of the parameters is made based on empirical analysis. This choice helps to optimize the performance of the classifier based on the complexity of the feature set.

Due to the limited amount of training data, a 5-fold stratified cross-validation (CV) is performed. Utilizing performance measures obtained from the confusion matrix, the effectiveness of the trained classifiers is assessed. The classifier outputs are divided into four categories using a confusion matrix: true positive (TP), false positive (FP), true negative (TN), and false negative (FN). Sensitivity, specificity, and accuracy are the performance measures computed, as given in Equations 1-3. By analyzing these performance measures, the classifiers' effectiveness in distinguishing between osteoporotic and healthy individuals based on the extracted features is evaluated.

$$Sensitivity = TP/TP + FN \quad (1)$$

$$Specificity = TN/(TN + FP) \quad (2)$$

$$Accuracy = (TP + TN)/(TP + TN + FP + FN) \quad (3)$$

4. Results

This section discusses the result analysis of the feature extraction methods. Significant features are filtered through feature selection techniques and used to train machine learning classifiers.

A. Feature extraction

The feature extraction methods enables to extract structural and texture features from the input data, capturing important patterns and characteristics. Three feature extraction methods are employed, namely LBP, GT and fractal dimension (FDTA).

Two experimental analyses are done in this research work. Firstly, the three feature extraction techniques are applied on the preprocessed images. This produces six features for LBP method, namely, $LBP_{1,8}\_energy$, $LBP_{1,8}\_entropy$, $LBP_{2,16}\_energy$, $LBP_{2,16}\_entropy$, $LBP_{3,24}\_energy$ and $LBP_{3,24}\_entropy$. $LBP_{n,m}\_feature$ denotes the feature measured from LBP image obtained with radius of n and neighbourhood of m pixels. Radii of 1, 2 and 3 pixels with 8, 16 and 24 neighbours are considered here. Gabor transform is applied on the preprocessed images to obtain 16 features, namely, $GT_{0,0.05}\_mean$, $GT_{0,0.05}\_std$, $GT_{0,0.4}\_mean$, $GT_{0,0.4}\_std$, $GT_{1,0.05}\_mean$, $GT_{1,0.05}\_std$, $GT_{1,0.4}\_mean$, $GT_{1,0.4}\_std$, $GT_{2,0.05}\_mean$, $GT_{2,0.05}\_std$, $GT_{2,0.4}\_mean$, $GT_{2,0.4}\_std$, $GT_{3,0.05}\_mean$, $GT_{3,0.05}\_std$, $GT_{3,0.4}\_mean$ and $GT_{3,0.4}\_std$. $GT_{n,m}\_mean$ and $GT_{n,m}\_std$ denotes the mean and standard deviation, respectively, calculated from the Gabor image with threshold n and frequency m. Four features are extracted using fractal dimension analysis, namely, $FDTA\_HurstCoef_1$, $FDTA\_HurstCoef_2$, $FDTA\_HurstCoef_3$ and $FDTA\_HurstCoef_4$. $FDTA\_HurstCoef_n$ denotes the n^{th} Hurst coefficient of the fractal dimension analysis of the preprocessed image.

In the second experimental analysis, the three feature extraction techniques (LBP, GT and FDTA) are applied on the wavelet-decomposed sub-images. The wavelet-decomposed sub-images are obtained by applying two-level Haar wavelet decomposition on the preprocessed images. The seven sub-images obtained are denoted as LH_1, HL_1, HH_1, LL_2, LH_2, HL_2 and HH_2. LBP, Gabor transform and fractal dimension features are extracted from the seven sub-images of wavelet decomposition, to obtain a total of 96 features. In this work, we aim to compare the performance of the classifiers using LBP, GT and FDTA features obtained from preprocessed images and those obtained from wavelet decomposed images. We investigate the impact of wavelet decomposition in the characterization of texture features from calcaneal bone radiographs.

Subsequently, feature selection methods are employed to filter the feature vectors by selecting the most relevant features, thereby enhancing the efficiency and interpretability of the classifiers.

B. Feature selection

An independent sample t-test is conducted to determine the p-value for each feature, and all significant features, with p-value less than 0.05, is grouped as Feature Set-1 (FS-1). From the statistical test results, it is observed that all the features obtained from the LBP analysis are significant, with p-value less than 0.05. Only one feature, $GT_{1,0.05}\_std$, is observed to be significant in the GT analysis. $GT_{1,0.05}\_std$ denotes the standard deviation calculated from the Gabor image with threshold 1 and frequency 0.05. In the FD analysis, two features are found to be significant, namely $FDTA\_HurstCoef_1$ and $FDTA\_HurstCoef_2$.

Next, a two-level wavelet decomposition transform (DWT) is done on the original images and then LBP, Gabor transform and fractal dimension features are extracted from each sub-band image. The sub-images are Low-Low, Low-High, High-Low and High-High sub-bands of level-2 DWT decomposition, denoted as LL_2, LH_2, HL_2 and HH_2 images, respectively. The respective sub-images of level-1 are LL_1, LH_1, HL_1 and HH_1, respectively.

The DWT analysis produced a total of 96 features, out of which 27 features are found significant using independent sample t-test. The 15 significant features of level-1 DWT are $LH_1\_LBP_{1,8}\_energy$, $LH_1\_LBP_{1,8}\_entropy$, $LH_1\_LBP_{2,16}\_energy$, $LH_1\_LBP_{2,16}\_entropy$, $LH_1\_FDTA\_HurstCoef_1$, $LH_1\_FDTA\_HurstCoef_2$, $HL_1\_LBP_{1,8}\_energy$, $HL_1\_LBP_{1,8}\_entropy$, $HL_1\_LBP_{2,16}\_energy$, $HL_1\_LBP_{2,16}\_entropy$, $HL_1\_FDTA\_HurstCoef_1$, $HL_1\_FDTA\_HurstCoef_2$, $HH_1\_LBP_{1,8}\_energy$, $HH_1\_LBP_{1,8}\_entropy$, and $HH_1\_FDTA\_HurstCoef_1$. $XX_i\_LBP_{n,m}\_feature$ denotes the feature measured from LBP image (with radius n and neighbourhood m pixels) of i^{th} level XX wavelet sub-image. Similarly, $XX_i\_FDTA\_HurstCoef_n$ denotes the n^{th} Hurst Coefficient of the fractal dimension analysis applied in i^{th} level XX wavelet sub-image. The remaining 12 significant features of level-2 DWT are $LH_2\_LBP_{1,8}\_energy$, $LH_2\_LBP_{1,8}\_entropy$, $LH_2\_LBP_{2,16}\_energy$, $LH_2\_LBP_{2,16}\_entropy$, $LH_2\_FDTA\_HurstCoef_1$, $HL_2\_LBP_{1,8}\_energy$, $HL_2\_LBP_{1,8}\_entropy$, $HL_2\_FDTA\_HurstCoef_1$, $HH_2\_GT_{3,0.5}\_mean$, $HH_2\_LBP_{2,16}\_energy$, $HH_2\_LBP_{2,16}\_entropy$, and $HH_2\_FDTA\_HurstCoef_1$. $XX_i\_GT_{n,m}\_feature$ denotes the feature measured from Gabor transform (with threshold n and frequency m) of i^{th} level XX wavelet sub-image.

Next, a second feature extraction method is implemented using forward feature selection method. Through the forward feature selection method, we obtain a feature vector for each classifier that consists of significant features associated with the highest accuracy. The feature vector obtained using forward feature selection method is denoted as FS-2. The objective of this approach is to determine the most relevant features for our analysis. Initially, we start with a set of features and employ a stepwise procedure that iteratively adds the best-performing feature, based on the highest increase in accuracy. The process continues until no further improvement in performance is observed.

For the three classifiers, three distinct feature vectors are obtained using forward feature selection technique. Since forward feature selection method selects the features based on their performance of a machine learning model, we obtain three distinct set of selected features for all the three classifiers, as shown in Table I. * denotes those features with p-value < 0.05. Table I shows that in the SVM classifier, the feature vector FS-2 comprise of five features, out of which four features exhibited a p-value below 0.05, indicating their statistical significance. For the KNN classifier, the feature vector FS-2 consists of 15 features, with five features displaying a p-value below 0.05. In the RF classifier, the feature vector FS-2 encompass 12 features, among which seven features possessed a p-value less than 0.05, as shown in Table I. Table I shows the set of features selected for each classifier. It demonstrates the importance of feature selection in improving the accuracy and interpretability of the classification models.

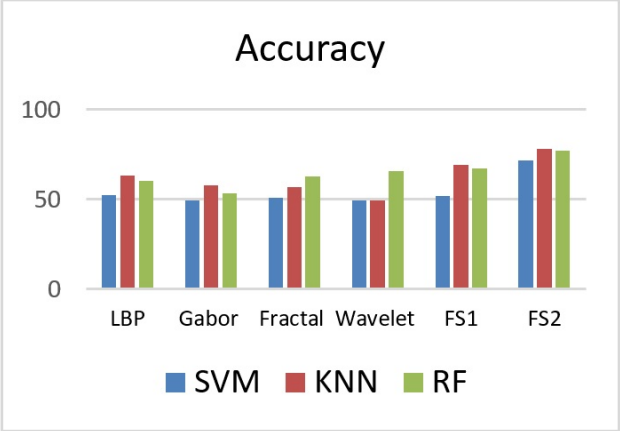

Figure 4. Five-fold cross validation accuracy of SVM, KNN and Random Forest classifiers trained using extracted texture feature sets.

C. Classification

In this work, feature extraction methods and feature selection methods are employed to construct feature vectors, which are then used to train three different classifiers, namely SVM, KNN and RF. The classifiers are evaluated based on their accuracy, which measures the overall correctness of the predictions. Figure 4 shows the 5-fold cross validation accuracy obtained by SVM, KNN and random forest classifiers on all feature sets. It is observed that FS-2 feature set shows the best 5-fold CV accuracy for all the three classifiers. Among these, KNN classifier trained with FS-2 feature set shows the best results.

Additionally, sensitivity and specificity, derived from the confusion matrix, provides insights into the classifiers' ability to correctly identify positive and negative instances. Figure 5 and Figure 6 show the sensitivity and specificity of the classifiers on feature sets. The best sensitivity measure is obtained for KNN classifier trained with LBP features and the SVM classifier trained with all wavelet features. But this comes with a trade-off with lower specificity values for the same classifiers, as shown in Figure 6. All three classifiers trained with FS-2 feature set shows the best trade-off values between the sensitivity and specificity measures.

Table II tabulates the accuracy, sensitivity and specificity values of KNN, SVM and random forest classifiers trained using different sets of trabecular texture features. The feature sets are LBP (6 features), Gabor transform (16 features), FDTA (4 features), wavelet transform (96 features), FS-1 (27 features) and FS-2 feature sets. The FS-2 feature sets, being derived using forward feature selection technique, have different feature measures for each classifier, as shown in Table I.

From Table II, it is observed that classifiers trained using wavelet derived features show better results than the features derived directly from the preprocessed images. This shows the ability of wavelet decomposition to extract

TABLE I. Five-fold cross validation (CV) results of features from forward feature selection (FS-2)

Classifier	Features	CV fold	CV score	Average CV score
KNN	$LH_1\_GT_{0,0.5}\_std$, $LH_1\_LBP_{1,8}\_energy$*, $LH_1\_LBP_{2,16}\_entropy$*, $HL_1\_GT_{2,0.5}\_std$, $HL_1\_FDTA\_HurstCoef_2$*, $HH_1\_GT_{1,0.5}\_std$, $HH_1\_LBP_{1,8}\_energy$*, $HH_1\_LBP_{2,16}\_entropy$, $HH_2\_GT_{0,0.5}\_std$, $HH_2\_GT_{2,0.5}\_std$, $HH_2\_LBP_{2,16}\_energy$*, $HL_1\_LBP_{2,16}\_energy$*, $HH_1\_GT_{0,0.5}\_std$, $HH_1\_GT_{2,0.5}\_std$, $HH_1\_LBP_{2,16}\_energy$,	1 2 3 4 5	0.68 0.89 0.66 0.88 0.77	0.78
SVM	$HH_1\_FDTA\_HurstCoef_1$, $HL_1\_LBP_{2,16}\_entropy$*, $HH_1\_LBP_{2,16}\_entropy$, $LH_1\_FDTA\_HurstCoef_1$*, $LH_2\_LBP_{2,16}\_entropy$*,	1 2 3 4 5	0.68 0.73 0.77 0.77 0.61	0.72
RF	$LH_1\_GT_{0,0.5}\_mean$, $LH_1\_FDTA\_HurstCoef_2$*, $HL_1\_GT_{2,0.5}\_mean$, $HL_1\_LBP_{1,8}\_entropy$*, $HH_1\_GT_{1,0.5}\_std$, $HH_1\_LBP_{1,8}\_energy$*, $HH_1\_LBP_{1,8}\_entropy$*, $HH_1\_FDTA\_HurstCoef_1$*, $HH_2\_LBP_{1,8}\_entropy$, $HL_1\_LBP_{1,8}\_energy$*, $LH_2\_LBP_{2,16}\_entropy$*, $HL_2\_GT_{1,0.5}\_std$,	1 2 3 4 5	0.78 0.78 0.88 0.77 0.66	0.77

TABLE II. Results obtained from the classifiers trained with different sets of features

Features	Classifiers	Sensitivity (%)	Specificity (%)	5-fold CV accuracy (%)
Local Binary Pattern	SVM	41.67	83.34	52.42
	KNN	91.67	50.00	63.01
	RF	50.00	75.00	60.28
Gabor Transform	SVM	66.67	50.00	49.09
	KNN	66.67	16.64	57.82
	RF	83.34	25.00	53.40
Fractal Dimension	SVM	41.67	75.00	50.76
	KNN	58.36	50.00	56.88
	RF	58.36	33.34	62.86
Wavelet Transform	SVM	91.67	25.00	49.09
	KNN	66.67	50.00	49.09
	RF	58.36	75.00	65.54
FS-1	SVM	83.34	50.00	51.60
	KNN	66.67	83.34	68.91
	RF	50.00	58.36	67.24
FS-2	SVM	75.24	67.70	71.75
	KNN	80.14	76.14	78.24
	RF	79.27	74.50	76.84

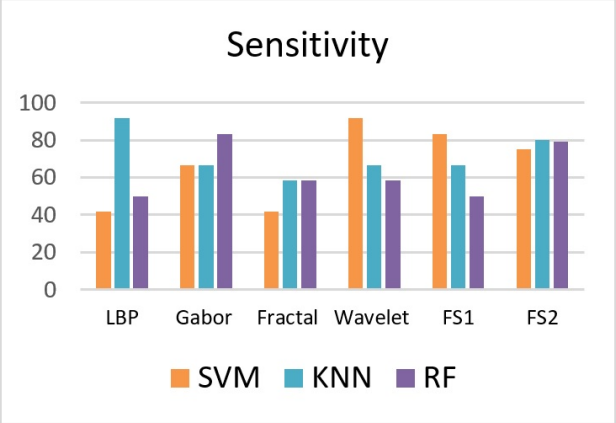

Figure 5. Sensitivity values of SVM, KNN and Random Forest classifiers trained using extracted texture feature sets.

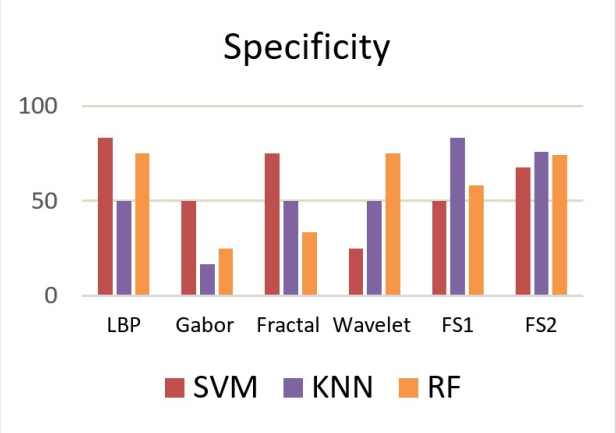

Figure 6. Specificity values of SVM, KNN and Random Forest classifiers trained using extracted texture feature sets.

contextual texture features of the trabecular bone, for better classification results. In general, the best results are obtained when the classifiers are trained with texture features selected by the feature selection methods, namely independent sample t-test and forward feature selection method. The feature set FS-2 outperforms other feature sets, indicating that forward feature selection is a better feature selection technique for identifying significant features in the calcaneal bone. Among the three classifiers, KNN trained using FS-2 features demonstrates the best performance. It achieves a 5-fold stratified cross-validation accuracy of 78.24%, with a sensitivity of 80.14% and specificity of 76.14%. This indicates that the classifier was able to accurately classify osteoporotic patients and healthy individuals, with a relatively high overall accuracy and a balanced sensitivity and specificity measure.

Figure 7 provides the Receiver Operating Characteristic (ROC) plots and the area under the ROC curve (AUC) of the 5-fold cross validation of KNN, RF and SVM classifiers trained using FS-2 feature set. The ROC of every fold along with the mean curve is plotted. The AUC values of the mean ROC of KNN, RF and SVM classifiers are 0.76, 0.73 and 0.73, respectively. This further illustrates the superior performance of the KNN classifier in the classification of osteoporotic bones. Overall, this work showcases the effectiveness of feature extraction, feature selection, and classifier training in analyzing and classifying osteoporosis based on the trabecular texture features.

5. Discussion

Osteoporosis, characterized by low bone mass and structural deterioration of bone tissue, leads to increased fracture risk. Traditional diagnostic methods like DXA are often expensive and not widely accessible, particularly in low-resource settings. This paper employs a low cost, lightweight and multi-faceted approach, combining wavelet decomposition for texture feature extraction, feature selection methods, and classical machine learning algorithms for classification. This comprehensive methodology enhances the robustness and accuracy of osteoporosis detection. The use of DWT is pivotal in our research. Wavelet decomposition allows the capture of both spatial and frequency information, making it superior for analyzing trabecular patterns in bone images. This method surpasses traditional image preprocessing techniques by isolating fine-grained textural features indicative of bone quality. DWT captures multi-resolution features, crucial for characterizing the complex trabecular structures. Previous studies have shown the potential of wavelets in medical imaging, but our work demonstrates their specific application in osteoporosis classification with a focus on calcaneal radiographs.

Feature selection is critical in reducing the dimensionality of the dataset and enhancing the classifier's performance. We have explored statistical analysis and forward feature selection techniques to identify the most relevant features from the wavelet-decomposed images. Statistical analysis helps in understanding the distribution and significance of individual features. Forward feature selection iteratively selects features that improve classifier performance, ensuring an optimal feature set. Three classical machine learning algorithms, SVM, KNN, and RF, are trained and evaluated for osteoporosis classification.

The outcomes of our proposed method are contrasted with those of existing studies that used the same dataset. Table III compares the results of the proposed method with related work using the same dataset. Palanivel et al. [27] computed Holder exponents, then Hausdorff dimensions are determined. Finally, lacunarity is computed and obtained accuracy of 59% with 59% sensitivity and 59% specificity. Riaz et al. [23] used Gabor filter bank, created using filters with four scales and four orientations. Afterwards, 1D-LBP histograms are acquired from which an accuracy of 72.71% is obtained. Palanivel et al. [24] utilized trabecular bone texture features which are extracted using the regularization and box-counting dimensions, and obtained accuracy of 55% with 59% sensitivity and 52% specificity. Bouzeboudja

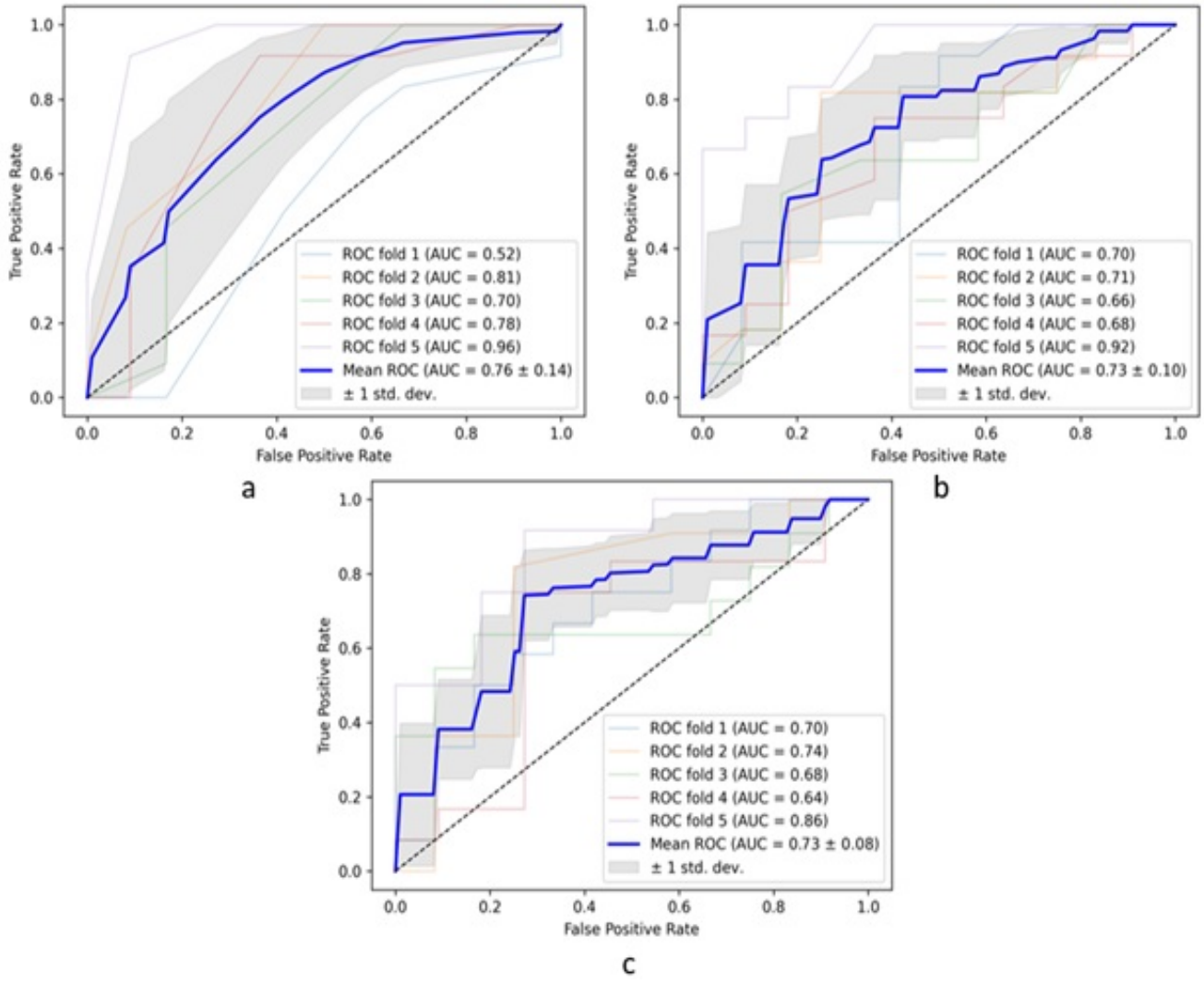

Figure 7. ROC plots and AUC values obtained for 5-fold cross validation of (a) KNN, (b) Random Forest, and (c) SVM classifiers.

et al. [28] computed features from multi-fractal spectrum, and achieved accuracy of 98.01%, with 97.26% sensitivity, 98.78% specificity and AUC of 98.37%.

Studies conducted by Yger [47] and Zheng and Makrogiannis [48] utilized the same dataset, consisting of 116 images. Their respective results showed an accuracy of 63.8% and 74.1%. Other studies have also utilized the same dataset in their work [22], [49], and [50]. However, they had included an additional blind data of 58 images, bringing the total dataset size to 174 images. By including these blind data, they were able to expand the dataset and potentially obtain more comprehensive insights and improved results compared to our proposed work. The availability of a larger dataset have provided a broader perspective and potentially enhanced the accuracy of their findings.

In addition to the present work, several other research works, including those conducted by [51],[52],[53],[54] have explored similar topics but utilized different datasets. Table IV compares the proposed method with related work using different dataset. Notably, the studies that incorporated larger datasets have shown promising results. The availability of a larger data pool has likely provided these studies with a more comprehensive representation of the underlying patterns and improved the reliability and generalizability of their findings.

In contrast to related work using complex algorithms, the proposed work aimed to produce a light-weight framework for screening of osteoporosis, using simple yet discriminatory feature extraction and selection techniques. The experimental results highlight the effectiveness of wavelet-derived features and the impact of feature selection on classification performance. Wavelet-derived features significantly outperform those extracted directly from pre-processed images, indicating the importance of capturing

TABLE III. Comparison with related work using calcaneal image data

Related work	Features used	Classifier	Dataset	Sensitivity (%)	Specificity (%)	Accuracy (%)
[47]	Wavelet Marginals-Haar	SVM	58 cases & 58 control	62.1	65.5	63.8
[48]	FD, wavelet transform, DFT, DCT, Gabor, LBP, Laws masks, edge	Random forest	58 cases & 58 control	74.10	74.10	74.1
[27]	Multifractal-based lacunarity analysis	SVM	58 cases & 58 control	59.00	59.00	59
[24]	Regularization dimension and box-counting dimension	SVM	58 cases & 58 control	59.00	52.00	55
[23]	Gabor filters and 1D local binary pattern (1D-LBP)	KNN	58 cases & 58 control	-	-	72.71
[49]	Histogram, GLCM, PCA	SVM	87 cases & 87 controls	97.70	95.40	96.60
[50]	Anisotropic discrete dual-tree wavelet transform	SVM	87 cases & 87 controls	-	93.10	91.90
[22]	Oriental fractal analysis	-	87 cases & 87 controls	72.00	71.00	71.80
[28]	Multi-fractal spectrum	LR	87 cases & 87 controls	97.26	98.78	98.01
[32]	Sparse analysis method	Deep learning	87 cases & 87 controls	-	-	72.67
Proposed method	**Features from Wavelet images using LBP, GT and FD**	**KNN**	**58 cases & 58 control**	**80.14**	**76.14**	**78.24**

detailed texture information. Previous studies have explored wavelets in other medical imaging contexts, but our work demonstrates their specific utility in analyzing trabecular bone patterns. Feature selection methods enhance classifier performance by eliminating redundant and irrelevant features. The KNN classifier, in particular, demonstrates superior accuracy compared to SVM and RF, emphasizing its potential as a reliable tool for osteoporosis screening.

In recent years, several research studies, including works by [30],[31],[32] have successfully employed deep learning techniques. These studies have leveraged the power of deep learning models to improve the accuracy and effectiveness of classification tasks. However, in our research, we did not utilize deep learning techniques due to the consideration that a substantial amount of data is typically required to train and effectively optimize deep learning models. Given the constraints of our dataset size, we opted for a machine learning technique that could yield meaningful results within the available data limitations. By acknowledging the previous works that utilized deep learning techniques, we highlight the potential of such methods in the classification of healthy and osteoporotic images. However, our work explored alternative approaches that can still provide valuable insights despite the challenges posed by limited data availability.

As discussed, a limitation of this work is the small dataset used. Conduction of clinical trials is required to validate the efficacy of this screening tool in diverse populations. As future work, mobile applications for the screening tool could be developed and integrated with clinical settings, in order to facilitate widespread use in remote and underserved areas.

6. Conclusion

The proposed work investigates the discrimination ability of wavelet decomposed calcaneal bone images for trabecular texture characterization and osteoporosis diagnosis. Our method was used to categorize 116 X-rays of bone

TABLE IV. Comparison with related work using different dataset

Related work	Features used	Classifier	Dataset	Sensitivity (%)	Specificity (%)	Accuracy (%)
[54]	1D-LBP	KNN	39 cases & 41 control	-	43.99	71.30
[51]	Fractional Brownian model and Rao geodesic distance	KNN	348 cases & 348 control	97.80	95.40	96.60
[53]	Cortical radiogrammetry and hLLBP	Logistic Regression	Distal radius 60 cases & 60 controls	81.70	76.70	79
[31]	Deep neural network architecture	Deep learning	186 cases & 186 controls	-	-	84.06
[52]	Cortical radiogrammetry, Run length matrices and Laws' masks	Neural network	Distal radius 58 cases & 59 controls	80	100	88.5
Proposed method	**Features from Wavelet images using LBP, GT and FD**	**KNN**	**58 cases & 58 control**	**80.14**	**76.14**	**78.24**

tissue, half of which were of patients with osteoporosis and the other half were of healthy individuals. There were four steps to the proposed method. The radiograph preprocessing in the first step was done to emphasize the trabecular bone network. The second step included feature extraction and texturing feature analysis. In the third stage, feature selection techniques were used to obtain significant features. In the last stage, three different classifiers were trained with the obtained significant features and the trained model was used classify osteoporotic patients and healthy subjects. Based on the results obtained, we can draw the following conclusions. The features extracted from wavelet transform images using LBP, GT, and FD proved to be valuable in the analysis of bone trabecular network. This suggests that both the orientation and fractal features play a significant role in this analysis. Furthermore, the feature vector obtained through forward feature selection demonstrated better performance compared to the feature vector obtained through independent sample t-test. This highlights the effectiveness of the forward feature extraction method in capturing relevant and discriminative features for the classification. Thus, the developed model can serve as a low cost, light weight and computationally less expensive tool for the classification of osteoporosis.

References

[1] S. K. Sabat, S. Panda, B. S. Sahoo, and P. Barik, "Prevalence of osteoporosis in india: A systematic review and meta-analysis," *International Journal of Health Sciences*, vol. 6, no. S4, pp. 10 154—-10 166, 2022.

[2] T. Sözen, L. Özışık, and N. Başaran, "An overview and management of osteoporosis," *European Journal of Rheumatology*, vol. 4, no. 1, pp. 46–56, 2017.

[3] T. D. Rachner, S. Khosla, and L. C. Hofbauer, "Osteoporosis: now and the future," *The Lancet*, vol. 377, no. 9773, pp. 1276—1287, 2011.

[4] N. Harvey, E. Dennison, and C. Cooper, "Osteoporosis: impact on health and economics," *Nature Reviews Rheumatology*, vol. 6, pp. 99—-105, 2010.

[5] A. S. Areeckal, M. Kocher, and S. S. David, "Current and emerging diagnostic imaging-based techniques for assessment of osteoporosis and fracture risk," *IEEE Reviews in Biomedical Engineering*, vol. 12, pp. 254–268, 2019.

[6] Y. Zhao, T. Zhao, S. Chen, X. Zhang, M. S. Sosa, J. Liu, X. Mo, X. Chen, M. Huang, S. Li *et al.*, "Fully automated radiomic screening pipeline for osteoporosis and abnormal bone density with a deep learning-based segmentation using a short lumbar mdixon sequence," *Quantitative Imaging in Medicine and Surgery*, vol. 12, no. 2, p. 1198, 2022.

[7] K. Fang, X. Zheng, X. Lin, and Z. Dai, "Unveiling osteoporosis through radiomics analysis of hip ct imaging," *Academic Radiology*, vol. 31, no. 3, pp. 1003–1013, 2024.

[8] R. Dhanagopal, R. Menaka, R. Suresh Kumar, P. Vasanth Raj, E. Debrah, and K. Pradeep, "Channel-boosted and transfer learning convolutional neural network-based osteoporosis detection from ct scan, dual x-ray, and x-ray images," *Journal of Healthcare Engineering*, vol. 2024, no. 1, p. 3733705, 2024.

[9] M. A. de Oliveira, R. Moraes, E. B. Castanha, A. S. Prevedello, J. Vieira Filho, F. A. Bussolaro, and D. G. Cava, "Osteoporosis screening: applied methods and technological trends," *Medical En-*

gineering & Physics, vol. 108, p. 103887, 2022.

[10] T. Feng, Y. Xie, W. Xie, Y. Chen, P. Wang, L. Li, J. Han, D. Ta, L. Cheng, and Q. Cheng, "Characterization of multi-biomarkers for bone health assessment based on photoacoustic physicochemical analysis method," *Photoacoustics*, vol. 25, p. 100320, 2022.

[11] A. Mithal, B. Bansal, S. C. Kyer, and P. Ebeling, "The asia-pacific regional audit-epidemiology, costs, and burden of osteoporosis in india 2013: A report of international osteoporosis foundation," *Indian Journal of Endocrinology and Metabolism*, vol. 18, no. 4, pp. 449—454, 2014.

[12] A. Rosholm, L. Hyldstrup, L. Bæksgaard, M. Grunkin, and H. H. Thodberg, "Estimation of bone mineral density by digital x-ray radiogrammetry: Theoretical background and clinical testing," *Osteoporosis International*, vol. 12, no. 11, pp. 961—969, 2001.

[13] J. Cui, C. L. Liu, R. Jennane, S. Ai, K. Dai, and T.-Y. Tsai, "A highly generalized classifier for osteoporosis radiography based on multiscale fractal, lacunarity, and entropy distributions," *Frontiers in Bioengineering and Biotechnology*, vol. 11, p. 1054991, 2023.

[14] K. A. Patil, K. M. Prashanth, and A. Ramalingaiah, "Classification of osteoporosis in the lumbar vertebrae using l2 regularized neural network based on phog features," *International Journal of Advanced Computer Science and Applications*, vol. 13, no. 4, 2022.

[15] J. Du, J. Wang, X. Gai, Y. Sui, K. Liu, and D. Yang, "Application of intelligent x-ray image analysis in risk assessment of osteoporotic fracture of femoral neck in the elderly," *Math Biosci Eng*, vol. 20, pp. 879–93, 2023.

[16] A. Dhanyavathi and M. Veena, "Osteoporosis detection and classification of femur x-ray images through spectral domain analysis using texture features," *International Journal of Advanced Computer Science and Applications*, vol. 14, no. 9, 2023.

[17] J. Massatith, N. Boonnam, and R. Hama, "Osteoporosis prognosis through machine learning analysis of x-ray films," in *2023 27th International Computer Science and Engineering Conference (ICSEC)*. IEEE, 2023, pp. 104–109.

[18] S. Dadsetan, G. Kitamura, D. Arefan, Y. Guo, K. Clancy, L. Yang, and S. Wu, "Machine learning and radiomics for osteoporosis risk prediction using x-ray imaging," *medRxiv*, pp. 2022–02, 2022.

[19] Y. Bo, G. Chen, L. Li, X. Tao, and R. Zhao, "Detection of osteoporosis using image processing methods," *Journal of Optics*, pp. 1–11, 2023.

[20] R. Widyaningrum, E. I. Sela, R. Pulungan, and A. Septiarini, "Automatic segmentation of periapical radiograph using color histogram and machine learning for osteoporosis detection," *International Journal of Dentistry*, vol. 2023, no. 1, p. 6662911, 2023.

[21] R. W. Liu, W. Ong, A. Makmur, N. Kumar, X. Z. Low, G. Shuliang, T. Y. Liang, D. F. K. Ting, J. H. Tan, and J. T. P. D. Hallinan, "Application of artificial intelligence methods on osteoporosis classification with radiographs—a systematic review," *Bioengineering*, vol. 11, no. 5, p. 484, 2024.

[22] K. Harrar, R. Jennane, K. Zaouchi, T. Janvier, H. Toumi, and E. Lespessailles, "Oriented fractal analysis for improved bone microarchitecture characterization," *Biomedical Signal Processing and Control*, vol. 39, pp. 474—-485, 2018.

[23] F. Riaz, R. Nemati, H. Ajmal, A. Hassan, E. Edifor, and R. Nawaz, "Osteoporosis classification using texture features." IEEE, 2019, pp. 575—-579.

[24] D. A. Palanivel, S. Natarajan, S. Gopalakrishnan, and R. Jennane, "Trabecular bone texture characterization using regularization dimension and box-counting dimension." IEEE, 2019, pp. 1047–1052.

[25] S. Zehani, A. Ouahabi, M. Oussalah, M. Mimi, and A. Taleb-Ahmed, "Bone microarchitecture characterization based on fractal analysis in spatial frequency domain imaging," *International Journal of Imaging Systems and Technology*, vol. 31, no. 1, pp. 141–159, 2021.

[26] K. Zheng, C. E. Harris, R. Jennane, and S. Makrogiannis, "Integrative blockwise sparse analysis for tissue characterization and classification," *Artificial Intelligence in Medicine*, vol. 107, p. 101885, 2020.

[27] D. A. Palanivel, S. Natarajan, S. Gopalakrishnan, and R. Jennane, "Multifractal-based lacunarity analysis of trabecular bone in radiography," *Computers in Biology and Medicine*, vol. 116, p. 103559, 2020.

[28] O. Bouzeboudja, B. Haddad, A. Taleb-Ahmed, S. Ameur, M. El Hassouni, and R. Jennane, "Multifractal analysis for improved osteoporosis classification," *Biomedical Signal Processing and Control*, vol. 80, p. 104225, 2023.

[29] M. Mebarkia, A. Meraoumia, L. Houam, and S. Khemaissia, "X-ray image analysis for osteoporosis diagnosis: From shallow to deep analysis," *Displays*, vol. 76, p. 102343, 2023.

[30] R. Lindsey, A. Daluiski, S. Chopra, A. Lachapelle, M. Mozer, S. Sicular, D. Hanel, M. Gardner, A. Gupta, R. Hotchkiss *et al.*, "Deep neural network improves fracture detection by clinicians," *Proceedings of the National Academy of Sciences*, vol. 115, no. 45, pp. 11 591–11 596, 2018.

[31] A. Kumar, R. C. Joshi, M. K. Dutta, R. Burget, and V. Myska, "Osteo-net: A robust deep learning-based diagnosis of osteoporosis using x-ray images," 2022, pp. 91–95.

[32] C. E. Harris and S. Makrogiannis, "Sparse analysis of block-boosted deep features for osteoporosis classification." IEEE, 2022, pp. 1––5.

[33] P. S. Dodamani and A. Danti, "Diagnosis of osteoporosis from x-ray images using automated techniques," in *2022 International Conference on Machine Learning, Big Data, Cloud and Parallel Computing (COM-IT-CON)*, vol. 1. IEEE, 2022, pp. 497–500.

[34] P. H. Basavaraja and S. Ganesarathinam, "An ensemble-of-deep learning model with optimally selected features for osteoporosis detection from bone x-ray images." *International Journal of Intelligent Engineering & Systems*, vol. 15, no. 5, 2022.

[35] K. A. Patil, K. M. Prashanth, and A. Ramalingaiah, "Law texture analysis for the detection of osteoporosis of lumbar spine (l1-l4) x-ray images using convolutional neural networks," *IAENG International Journal of Computer Science*, vol. 50, no. 1, pp. 71–85, 2023.

[36] Y.-P. Chen, W. P. Chan, H.-W. Zhang, Z.-R. Tsai, H.-C. Peng, S.-W. Huang, Y.-C. Jang, and Y.-J. Kuo, "Automated osteoporosis classification and t-score prediction using hip radiographs via

deep learning algorithm," *Therapeutic Advances in Musculoskeletal Disease*, vol. 16, p. 1759720X241237872, 2024.

[37] S. Kim, B. R. Kim, H.-D. Chae, J. Lee, S.-J. Ye, D. H. Kim, S. H. Hong, J.-Y. Choi, and H. J. Yoo, "Deep radiomics–based approach to the diagnosis of osteoporosis using hip radiographs," *Radiology: Artificial Intelligence*, vol. 4, no. 4, p. e210212, 2022.

[38] K. Hidjah, A. Harjoko, M. E. Wibowo, and R. R. Shantiningsih, "Periapical radiograph texture features for osteoporosis detection using deep convolutional neural network," *International Journal of Advanced Computer Science and Applications*, vol. 13, no. 1, pp. 223–232, 2022.

[39] D.-J. Tsai, C. Lin, C.-S. Lin, C.-C. Lee, C.-H. Wang, and W.-H. Fang, "Artificial intelligence-enabled chest x-ray classifies osteoporosis and identifies mortality risk," *Journal of Medical Systems*, vol. 48, no. 1, p. 12, 2024.

[40] M. Ü. ÖZİÇ, M. Tassoker, and F. Yuce, "Fully automated detection of osteoporosis stage on panoramic radiographs using yolov5 deep learning model and designing a graphical user interface," *Journal of Medical and Biological Engineering*, vol. 43, no. 6, pp. 715–731, 2023.

[41] M. Tassoker, M. U. Ozic, and F. Yuce, "Prediction of osteoporosis through deep learning algorithms on panoramic radiographs," 2022.

[42] S. Kumar, P. Goswami, and S. Batra, "Enriched diagnosis of osteoporosis using deep learning models," *International Journal of Performability Engineering*, vol. 19, no. 12, p. 824, 2023.

[43] A. Hadid, J. Ylioinas, M. Bengherabi, M. Ghahramani, and A. Taleb-Ahmed, "Gender and texture classification: A comparative analysis using 13 variants of local binary patterns," *Pattern Recognition Letters*, vol. 68, pp. 231–238, 2015.

[44] L. Pothuaud, C. Benhamou, P. Porion, E. Lespessailles, R. Harba, and P. Levitz, "Fractal dimension of trabecular bone projection texture is related to three-dimensional microarchitecture," *Journal of Bone and Mineral Research*, vol. 15, no. 4, pp. 691–699, 2000.

[45] O. Regniers, L. Bombrun, V. Lafon, and C. Germain, "Supervised classification of very high resolution optical images using wavelet-based textural features," *IEEE Transactions on Geoscience and Remote Sensing*, vol. 54, no. 6, pp. 3722–3735, 2016.

[46] A. Jović, K. Brkić, and N. Bogunović, "A review of feature selection methods with applications," in *38th international convention on information and communication technology, electronics and microelectronics (MIPRO)*. IEEE, 2015, pp. 1200–1205.

[47] F. Yger, "Challenge ieee-isbi/tcb: application of covariance matrices and wavelet marginals," *arXiv preprint arXiv:1410.2663*, 2014.

[48] K. Zheng and S. Makrogiannis, "Bone texture characterization for osteoporosis diagnosis using digital radiography," in *2016 38th Annual International Conference of the IEEE Engineering in Medicine and Biology Society (EMBC)*. IEEE, 2016, pp. 1034–1037.

[49] A. Singh, M. K. Dutta, R. Jennane, and E. Lespessailles, "Classification of the trabecular bone structure of osteoporotic patients using machine vision," *Computers in biology and medicine*, vol. 91, pp. 148–158, 2017.

[50] H. Oulhaj, M. Rziza, A. Amine, H. Toumi, E. Lespessailles, M. El Hassouni, and R. Jennane, "Anisotropic discrete dual-tree wavelet transform for improved classification of trabecular bone," *IEEE transactions on medical imaging*, vol. 36, no. 10, pp. 2077–2086, 2017.

[51] M. El Hassouni, A. Tafraouti, H. Toumi, E. Lespessailles, and R. Jennane, "Fractional brownian motion and rao geodesic distance for bone x-ray image characterization," *IEEE Journal of Biomedical and Health Informatics*, vol. 21, no. 5, pp. 1347–1359, 2016.

[52] A. Areeckal, N. Jayasheelan, J. Kamath, S. Zawadynski, M. Kocher, and S. David S, "Early diagnosis of osteoporosis using radiogrammetry and texture analysis from hand and wrist radiographs in indian population," *Osteoporosis International*, vol. 29, pp. 665–673, 2018.

[53] A. S. Areeckal, J. Kamath, S. Zawadynski, M. Kocher *et al.*, "Combined radiogrammetry and texture analysis for early diagnosis of osteoporosis using indian and swiss data," *Computerized Medical Imaging and Graphics*, vol. 68, pp. 25–39, 2018.

[54] L. Houam, A. Hafiane, A. Boukrouche, E. Lespessailles, and R. Jennane, "One dimensional local binary pattern for bone texture characterization," *Pattern Analysis and Applications*, vol. 17, pp. 179–193, 2014.